

Figure 7 A small-signal equivalent circuit model of a RF SOI MOSFET under CSB configuration. [Color figure can be viewed at wileyonlinelibrary.com]

method using (7)–(11). From this method, V_{gs} -dependent extrinsic capacitance data are extracted in Figure 6. The C_{gdo} and C_{gso} data are almost constant in the negative V_{gs} , and rapidly increase in the positive V_{gs} due to the weak inversion channel formation. The data of C_{gb} largely increase with more negative V_{gs} because the channel depletion region is shrunk due to the rise of accumulated holes in the channel. As source and drain junction area gradually increases due to the shrinkage of the channel depletion region, C_{jso} and C_{jdo} data slightly increase with more negative V_{gs} . The values of C_{bo} are nearly independent of V_{gs} because of the source-drain lateral coupling capacitance existing in the buried oxide region.

Using the extracted C_{bo} , small-signal equivalent circuit modeling using Figure 7 under CSB configuration is carried out in the saturation region. To extract C_{jd} , the following equation is derived in the LF region.

$$C_{jd} + C_{bo} \approx (1/\omega)\text{Imag}(Y_{22}^c + Y_{12}^c)_{LF} \quad (12)$$

where Y^c -parameters are obtained by subtracting the extracted R_d from measured S -parameters.

The value of C_{jd} is obtained by subtracting the extracted C_{bo} from (12). Other model parameters except C_{bo} and C_{jd} in Figure 7 are extracted using a previous direct extraction method [6,7].

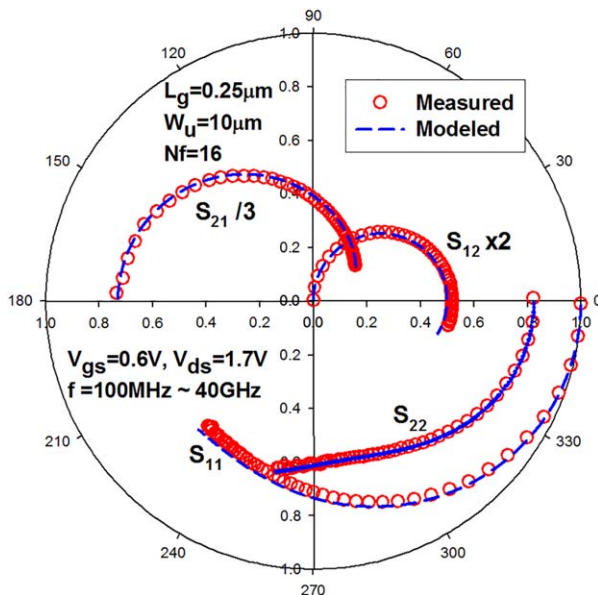


Figure 8 Comparison between modeled and measured S -parameters under CSB configuration at $V_{gs} = 0.6$ V and $V_{ds} = 1.7$ V. [Color figure can be viewed at wileyonlinelibrary.com]

The extraction accuracy of C_{bo} is verified by observing excellent agreements between modeled and measured S -parameters up to 40 GHz as shown in Figure 8.

3. CONCLUSION

A new and direct extraction method is proposed to get rid of the problem of previous methods due to C_{bo} in extracting extrinsic capacitances of RF SOI MOSFETs. This method is based on the LF extraction equations combining Y -parameters of two CSB and CGB AC equivalent circuits in the “off” state bias. Using this method, physically acceptable V_{gs} -dependent capacitance data are directly extracted. Accurate small-signal equivalent circuit modeling is carried out using the extracted C_{bo} in the saturation region under CSB configuration.

ACKNOWLEDGMENT

This research was supported by Basic Science Research Program through the National Research Foundation of Korea(NRF) funded by the Ministry of Education (No. NRF-2015R1D1A1A01059866)

REFERENCES

1. K.B. Ali, C.R. Neve, A. Gharsallah, and J.P. Raskin, RF performance of SOI CMOS technology on commercial 200-mm enhanced signal integrity high resistivity SOI substrate, *IEEE Trans Electron Dev* 61 (2014), 722–728.
2. S.F. Tin, A.A. Osman, K. Mayaram, and C. Hu, A simple subcircuit extension of the BSIM3v3 model for CMOS RF design, *IEEE J Solid State Circuits* 35 (2000), 612–624.
3. S. Lee and H.K. Yu, A semianalytical parameter extraction of a SPICE BSIM3v3 for RF MOSFET’s using S -parameters, *IEEE Trans Microwave Theory Tech* 48 (2000), 412–416.
4. S. Lee, A direct method to extract RF MOSFET model parameters using common source-gate and source-drain configurations, *Microwave Opt Technol Lett* 50 (2008), 915–917.
5. J.Y. Kim, M.K. Choi, and S. Lee, A “thru-short-open” de-embedding method for accurate on-wafer RF measurements of nano-scale MOSFETs, *J Semicond Technol Sci* 12 (2012), 53–58.
6. S. Lee, An accurate RF extraction method for resistances and inductances of sub-0.1 μ m CMOS transistors, *Electron Lett* 41 (2005), 1325–1327.
7. S. Lee, Direct extraction technique for a small-signal MOSFET equivalent circuit with substrate parameters, *Microwave Opt Technol Lett* 39 (2003), 344–347.

© 2016 Wiley Periodicals, Inc.

SMALL-SIZE DUAL-WIDEBAND IFA FRAME ANTENNA CLOSELY INTEGRATED WITH METAL CASING OF THE LTE SMARTPHONE AND HAVING DECREASED USER’S HAND EFFECTS

Kin-Lu Wong and Yu-Ching Wu

Department of Electrical Engineering, National Sun Yat-sen University, Kaohsiung 80424, Taiwan; Corresponding author: wongkl@ema.ee.nsysu.edu.tw

Received 14 May 2016

ABSTRACT: A small-size frame antenna based on the inverted-F antenna (IFA) structure to cover 824~960 and 1710~2690 MHz for the LTE operation in the metal-casing smartphone is presented. The antenna uses a short frame section of 53 mm (about 0.16 wavelength at 900 MHz) along the short edge of the metal casing as the IFA’s radiating strip. The short frame section is closely integrated with the metal casing with a 2-mm uniform gap and is easily fit within the short edge thereof. The frame section is connected to a feed circuit board (FCB), on which

the IFA's shorting strip, feeding strip and matching network are disposed, to achieve the desired dual-wideband operation. The FCB does not occupy the planar space on the metal casing and the system circuit board as well. In this regard, the occupied space of the antenna including the radiating frame section and the FCB in the smartphone is minimized. With the proposed antenna structure, effects of the user's hand on the antenna performance are also minimized, mainly because the small size of the antenna leads to no gaps along two long side edges of the metal-casing smartphone. Details of the antenna structure and its working principle are addressed, and experimental results of the antenna are presented and discussed. © 2016 Wiley Periodicals, Inc. *Microwave Opt Technol Lett* 58:2853–2858, 2016; View this article online at wileyonlinelibrary.com. DOI 10.1002/mop.30165

Key words: mobile antennas; smartphone antennas; inverted-F antennas; frame antennas; LTE antennas

1. INTRODUCTION

Metal casing can enhance the robustness of the modern slim tablet device such as the smartphone. The metal-casing structure, however, will cause significant effects on the internal antenna embedded in the tablet device and degrade the radiation performance of the antenna. In order to decrease the negative effects of the metal casing, the metal-frame antenna based on the inverted-F antenna (IFA) structure to integrate with the metal casing of the tablet device has been shown to be promising [1–5]. However, since the metal-frame antenna is disposed on the outer surface of the device casing, it is easy to be touched by the user's hand. This will cause significant effects on the antenna performance. For example, in the IFA-based frame antenna reported in Refs. [4,5], the antenna length is required to be about 84 mm [4] or 94 mm [5], which is at least about 0.25 wavelength at 900 MHz for the long term evolution (LTE) operation. Such a long frame antenna cannot fit within the short edge of the modern smartphone and the radiating frame will extend to two long side edges thereof, which makes it easily to be touched by the user's hand. In this case, there will be strong user's hand effects on the antenna performance.

In this paper, a small-size IFA frame antenna for the LTE operation in the metal-casing smartphone is presented. The required frame length of the antenna is 53 mm only, which is about 0.16 wavelength at 900 MHz and is much less than that reported in Refs. [4,5]. The much shorter frame length for the proposed antenna is owing to only a single resonant frame section needed for the dual-wideband operation. This is in contrast to the design of using two resonant frame sections [4,5] for the dual-wideband operation, in which the longer and shorter frame sections contribute respectively to the antenna's low and high bands. However, with the use of only one single short resonant frame section in the metal-casing smartphone, the generation of two wide operating bands for the LTE operation is a design challenge.

In order to achieve wider bandwidths of the antenna's low and high bands, a feed circuit board (FCB) with the feeding, shorting, and tuning strips disposed thereon is connected to the frame section to form the IFA frame antenna. The FCB does not occupy the planar space on the metal casing and the system circuit board, so that the occupied space of the antenna including the radiating frame section and the FCB in the smartphone is minimized [5]. With the proposed structure, the IFA frame antenna can generate its fundamental and first higher-order resonant modes in the desired low and high bands, respectively. By further embedding a wideband matching network [6] in the feeding strip, additional resonances close to the two resonant

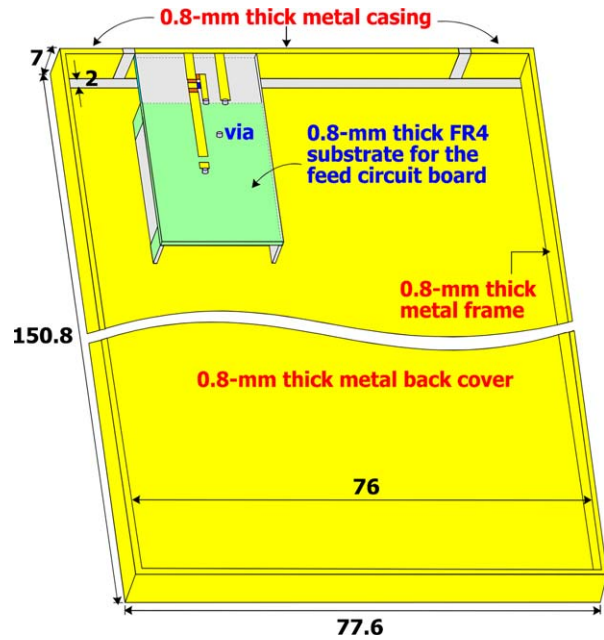


Figure 1 Geometry of the small-size dual-wideband IFA frame antenna for the LTE metal-casing smartphone. [Color figure can be viewed at wileyonlinelibrary.com]

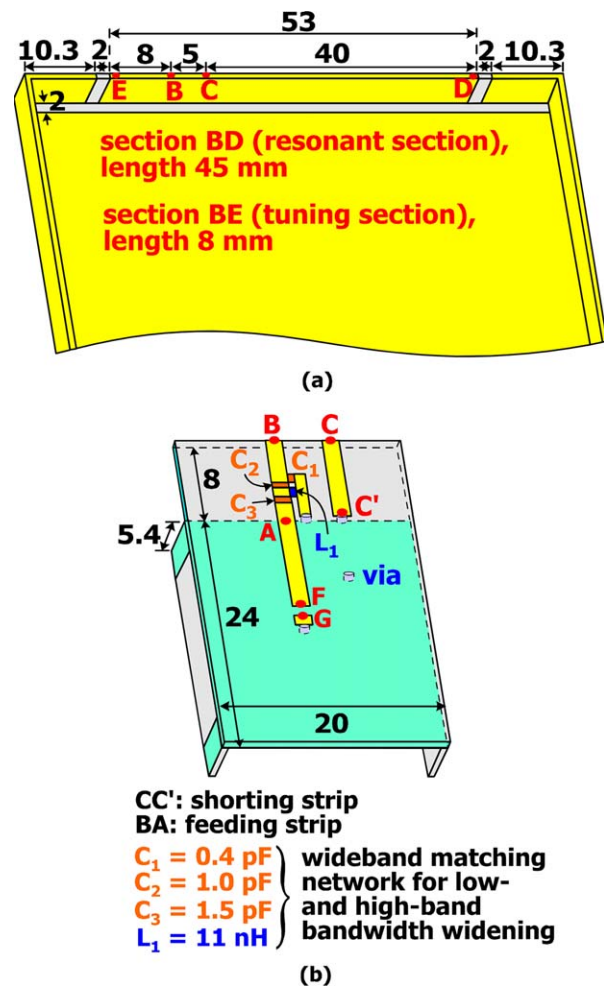


Figure 2 (a) The antenna without the FCB. (b) The feed circuit board. [Color figure can be viewed at wileyonlinelibrary.com]

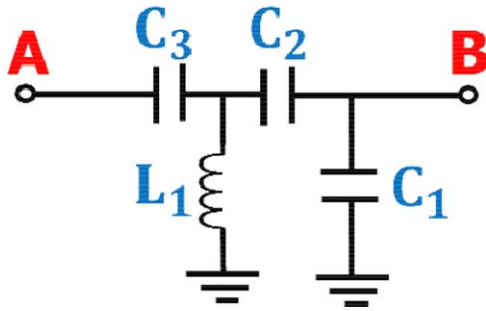


Figure 3 Equivalent circuit of the matching network disposed on the feed circuit board. [Color figure can be viewed at wileyonlinelibrary.com]

modes can be generated to greatly widen the antenna's low and high bands to cover the LTE operation in 824~960 and 1710~2690 MHz.

In addition, with the dual-wideband obtained, the antenna's radiating frame section can be easily placed at the short edge of the metal casing. That is, the radiating frame section will not be touched by the user's hand. Effects of the user's hand on the antenna performance are hence expected to be small. The antenna structure is described in detail in this study. Experimental results of the fabricated prototype are presented. The working principle of the antenna is also analyzed.

2. ANTENNA STRUCTURE AND EXPERIMENTAL RESULTS

2.1. Antenna Structure

Figure 1 shows the geometry of the small-size dual-wideband IFA frame antenna for the LTE metal-casing smartphone. The metal casing is assumed to have a reasonable size of $150.8 \times 77.6 \times 7 \text{ mm}^3$ for the modern slim smartphone. Along the top edge of the metal back cover of the metal casing, there is a narrow metal clearance of 2 mm in width. Note that the metal casing in the study is fabricated using a two-side copper-coated FR4 substrate of thickness 0.8 mm. That is, the metal casing

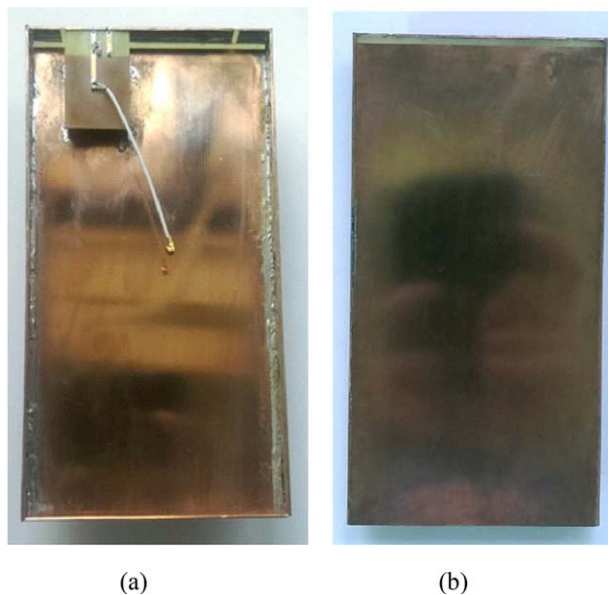


Figure 4 Photos of (a) the fabricated antenna and (b) back view of the metal casing. [Color figure can be viewed at wileyonlinelibrary.com]

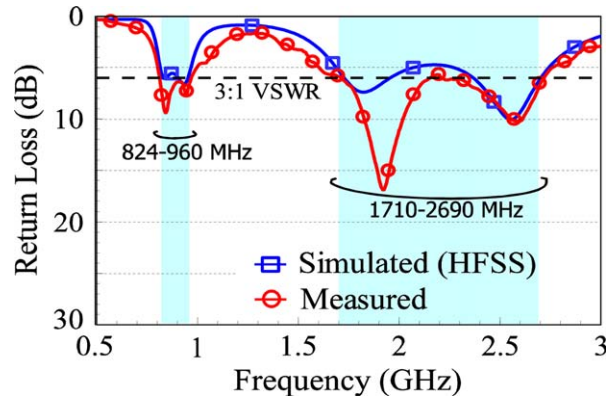


Figure 5 Measured and simulated return losses for the fabricated antenna. [Color figure can be viewed at wileyonlinelibrary.com]

including the metal back cover and the metal frame along four edges thereof has a thickness of 0.8 mm. Also, in this case, at the 2-mm metal clearance, there is a 0.8-mm thick FR4 substrate therein.

The antenna has an IFA structure [7] comprising the metal frame section DE of length 53 mm [see Fig. 2(a)] as the IFA's radiating strip and the FCB shown in Figure 2(b) on which the IFA's feeding and shorting strips are disposed thereon. The metal frame section DE is centered at the short edge and is spaced 10.3 mm away from the two nearby corners. For the metal frame section DE, the section BD of length 45 mm is the resonant section to generate the IFA's fundamental and higher-order resonant modes, while the section BE of length 8 mm is a tuning section only. The short tuning section fine tunes the IFA's excited higher-order resonant mode to occur the desired high band and does not contribute to the resonant path of the antenna.

The FCB is also made from a 0.8-mm thick FR4 substrate. The FCB has a no-ground region of width 8 mm to accommodate the feeding strip (section BA), the shorting strip (section CC'), and the matching network (C_1 , C_2 , C_3 , L_1). Figure 3 shows the equivalent circuit of the matching network, which creates additional resonances in close proximity to the two resonant modes excited in the antenna's low and high bands to widen the bandwidths thereof. Details of the matching network effects will be analyzed with the aid of Figures 9 and 10 in Section 3. The FCB does not occupy the planar space on the metal

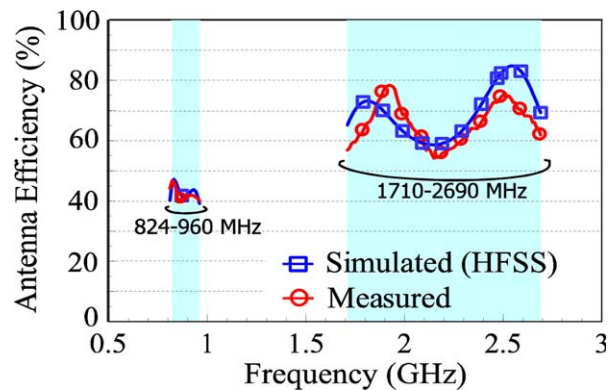


Figure 6 Measured and simulated antenna efficiencies for the fabricated antenna. [Color figure can be viewed at wileyonlinelibrary.com]

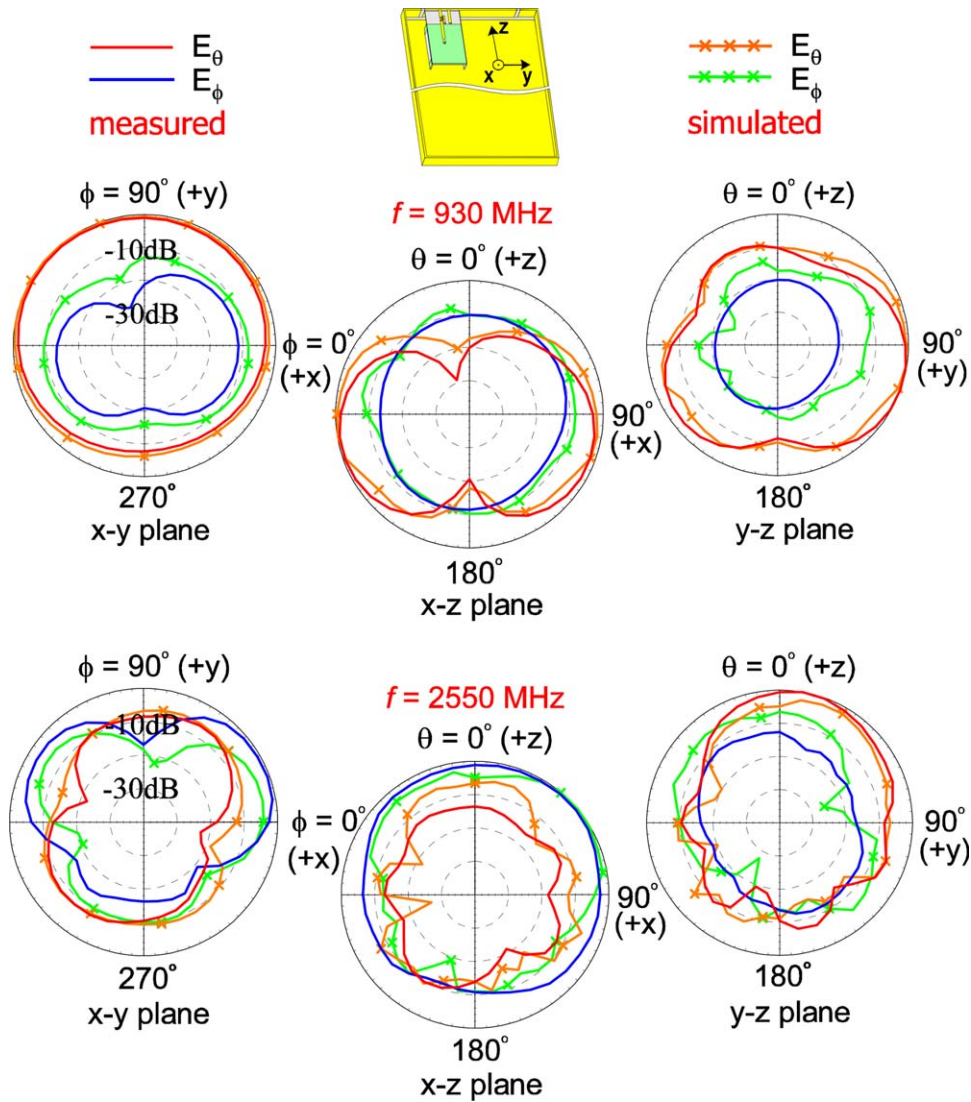


Figure 7 Measured and simulated radiation patterns for the fabricated antenna. [Color figure can be viewed at wileyonlinelibrary.com]

back cover, yet it is grounded to the metal back cover through four grounding strips. Note that the ground region of the FCB is selected to be $24 \times 20 \text{ mm}^2$ in this study, however other ground dimensions can be selected. For example, a much small ground

region of the FCB can be selected, so that the FCB can have a smaller size to be disposed between the small space between the metal frame and the system circuit board in modern slim smartphone.

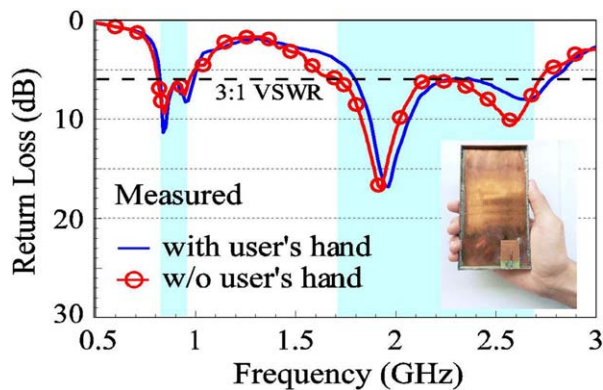


Figure 8 Measured return loss with user's hand presence; the antenna disposed at the bottom edge of the smartphone. [Color figure can be viewed at wileyonlinelibrary.com]

2.2. Experimental Results

Figure 4 shows the photos of the fabricated antenna and back view of the metal casing. The measured and simulated return losses for the fabricated antenna are shown in Figure 5. The two colored frequency regions in the figure denote the desired low band (824~960 MHz) and high band (1710~2690 MHz). Dual-resonances are observed in both low and high bands, which lead to widened bandwidths thereof. The measured data are in fair agreement with the simulated results obtained using the full-wave high frequency structure simulator (HFSS) version 16 [8]. Note that the measured return losses for frequencies in the low and high bands are generally better than 6 dB (3:1 VSWR). Figure 6 shows the measured and simulated antenna efficiencies for the fabricated antenna. Fair agreement between the measurement and simulation is also seen. The antenna efficiencies include the mismatching losses. The measured antenna efficiencies are about 40~47% in the low band and 55~78% in the high band.

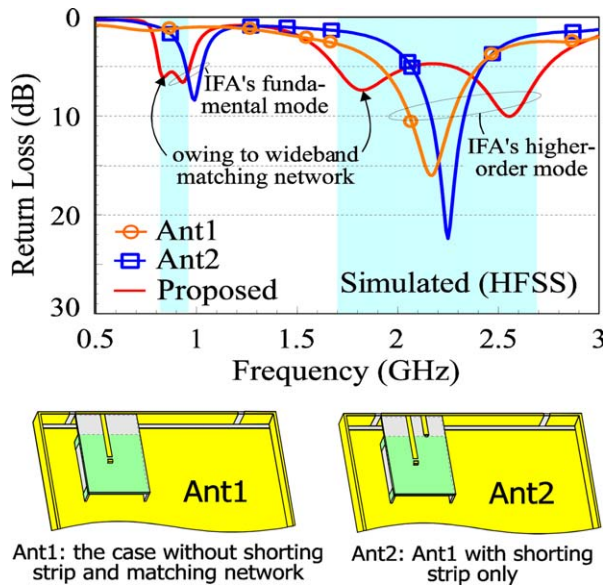


Figure 9 Simulated return loss for the proposed antenna, the case without the shorting strip and matching network in the feeding strip (Ant1), and Ant1 with the shorting strip only (Ant2). [Color figure can be viewed at wileyonlinelibrary.com]

The obtained antenna efficiencies are acceptable for practical mobile communication applications [9,10].

For the radiation patterns, the measured and simulated results are plotted in Figure 7. Results for two frequencies at 930 and 2550 MHz are shown, and fair agreement between measurement and simulation is also obtained. At 930 Hz, the radiation pattern in the x - y plane (azimuthal plane) is close to omnidirectional and the E_θ pattern in the x - z plane (elevation plane orthogonal to the metal casing) shows an inverted-8 figure. These characteristics are related to the excited surface currents on the metal casing, which also contributes to the antenna radiation. This is similar to the observation that the system ground plane of the smartphone will also contribute to the antenna radiation [11]. In the y - z plane (elevation plane parallel to the metal casing), stronger radiation is seen in the $+y$ direction. This is mainly because the open end of the frame section BD is to the $+y$ direction, which will make the excited surface current distribution stronger to the $+y$ direction.

At 2550 MHz, a representative frequency in the antenna's high band, much stronger radiation to the $+y$ direction is seen in the x - y and y - z planes. This behavior is similar to that observed at 930 MHz and is mainly related to the open end of the frame section BD pointing to the $+y$ direction. In the x - z plane, much stronger radiation in the $+z$ direction is seen at 2550 MHz, different from that seen at 930 MHz. This is mainly because the metal casing at higher frequencies functions more like a reflector than a radiator.

Experimental results of the user's hand holding the metal casing with the antenna disposed at the bottom edge of the smartphone are also presented in Figure 8. Note that the case with the antenna disposed at the top short edge is not studied, since the effect is expected to be small because the user's hand in normal conditions will not cover or touch the antenna at the top short edge. It is seen that both the measured results for the cases with and without the users' hand presence are generally the same. That is, very small effects on the impedance matching of the antenna owing to the user's hand presence are observed.

This agrees with the expectation, since the radiating frame section ED of the antenna has a short length and is not touched by the user's hand. This feature will be attractive for the proposed IFA frame antenna for practical applications.

3. WORKING PRINCIPLE OF THE ANTENNA

To analyze the working principle, Figure 9 shows the simulated return loss for the proposed antenna, the case without the shorting strip and matching network in the feeding strip (Ant1), and Ant1 with the shorting strip only (Ant2). Antenna structures of Ant1 and Ant2 are also shown in the figure. Ant1 can be considered as a simple monopole antenna. In this case, there is only one resonant mode successfully excited at about 2.2 GHz. No resonant mode is excited in the desired low band. By adding the shorting strip to form an IFA frame antenna (Ant2), a resonant mode at about 1 GHz is generated, with the resonant mode in the high band slightly shifted to higher frequencies.

Then, by further adding the wideband matching network in the feeding strip of the antenna, additional resonances in the low and high bands are created to widen the bandwidths thereof. Note that although the impedance matching for frequencies in the low and high bands are not all better than 6 dB for the antenna, the simulated and measured antenna efficiencies of the antennas as shown in Figure 6 are all better than 40% in the low band and 55% in the high band, acceptable for smartphone applications.

The wideband matching network comprises four elements as shown in Figures 2(b) and 3. As shown in Figure 10, when only the parallel chip capacitor C_1 (0.4 pF) and the series chip capacitor C_2 (1.0 pF) are added in Ant2 to form Ant2a (see the antenna structure in the figure), an additional resonance at about 1.7 GHz can be generated, with no additional resonance created in the low band. In this case, C_1 and C_2 also function like a low-pass matching circuit. By further adding the parallel chip inductor L_1 (11 nH) and the series chip capacitor C_3 (1.5 pF),

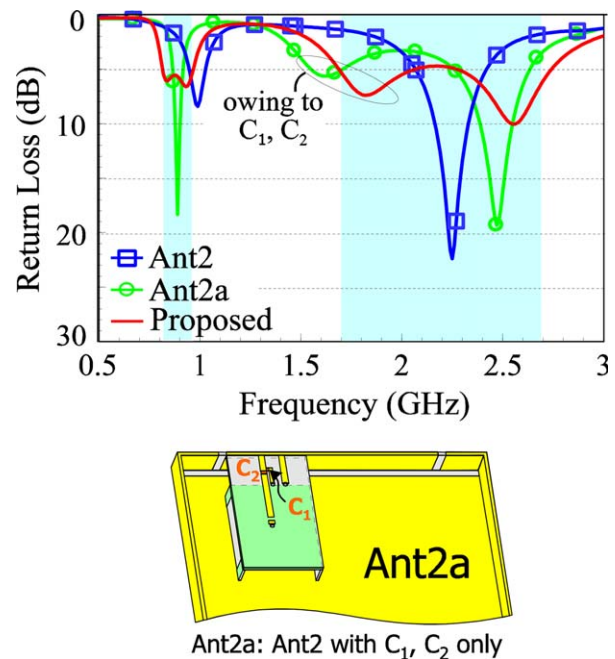


Figure 10 Simulated return loss for Ant2, Ant2 with C_1 and C_2 in the matching network (Ant2a), and proposed antenna (Ant2 with C_1 , C_2 , L_1 and C_3 in the matching network). [Color figure can be viewed at wileyonlinelibrary.com]

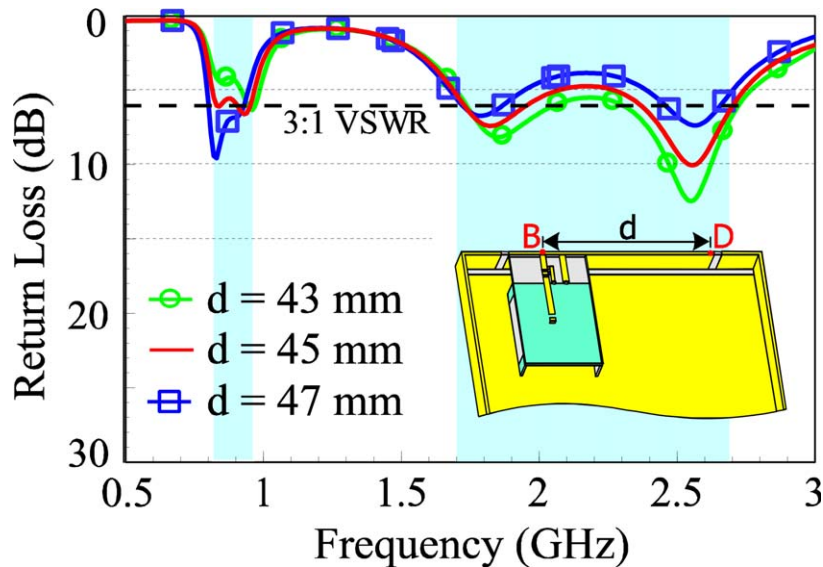


Figure 11 Simulated return loss as a function of the frame length d of the section BD. [Color figure can be viewed at wileyonlinelibrary.com]

both performing like a high-pass matching circuit, an additional resonance to widen the low-band bandwidth is generated. Hence, with the proposed matching network, dual-wideband operation of the antenna can be obtained. The results shown in Figure 10 can provide as a design guideline for achieving the bandwidth enhancement of the antenna's low and high bands.

Also note that since the section BD is the resonant frame section to generate the antenna's fundamental and higher-order resonant modes for the antenna, effects of its length variations on the antenna performance are studied. Figure 11 shows the simulated return loss as a function of the frame length d of the section BD. Results for the length d varied from 43 to 47 mm are presented. The matching network remains the same for the three cases. Note that for each case, the antenna's frame section is adjusted to be centered at the shorted edge and spaced 2 mm to nearby frame sections and metal back cover. That is, the antenna's frame section remains closely integrated with the metal casing. It is seen that with a decrease in the length d , the resonant modes in the low band are shifted to higher frequencies. On the other hand, the impedance matching in the high band is improved with the decreasing length d . The resonant frequencies in the high band, however, are very slightly affected. The obtained results indicate that the frame length d has a larger effect on the resonant frequency of the antenna's fundamental resonant mode than that of the antenna's higher-order resonant mode. It is hence suggested that the proper length of the frame section is better to be selected first for the antenna design. Then, the proper matching network can be determined by following the design guideline in the discussion of Figure 10.

4. CONCLUSION

A small-size IFA frame antenna for the LTE metal-casing smartphone has been proposed. The IFA frame antenna can provide two wide bands of 824~960 and 1710~2690 MHz and closely integrate with the metal casing of the smartphone. Owing to the small size of the antenna, decreased user's hand effects on the antenna performance has been obtained. Since the proposed antenna uses a frame section of the metal casing as the IFA's radiator and a FCB spaced away from the metal back

cover to accommodate the IFA's feeding strip, shorting strip and matching network, the antenna's occupied space inside the smartphone is reduced to be minimum. Acceptable radiation characteristics of the antenna have also been obtained. The proposed antenna is especially suitable for applications in the metal-casing smartphone for the LTE operation.

REFERENCES

1. R.J. Hill, R.W. Schlub, and R. caballero, Antennas for handheld electronic devices with conducting bevels, U.S. Patent No. 7924231 B2, 2011.
2. P. Bevelacqua, Dynamically adjustable antenna supporting multiple antenna modes, U.S. Patent No. 8982002 B2, Mar. 17, 2015.
3. A.J. Golko and D.W. Jarvis, Peripheral electronic device housing members with gaps and dielectric coatings, U.S. Patent No. 8947303 B2, Feb. 3, 2015.
4. H. Chen and A. Zhao, LTE antenna design for mobile phone with metal frame, *IEEE Antenna Wirel Propag Lett* 15, in press.
5. K. L. Wong and C. Y. Tsai, IFA-based metal-frame antenna without ground clearance for the LTE/WWAN operation in the metal-casing tablet computer, *IEEE Trans Antennas Propag* 64 (2016), 53–60.
6. K.L. Wong and Z.G. Liao, Small-size dual-wideband monopole antenna with inductive and capacitive feeding branches for long term evolution tablet computer application, *Microwave Opt Technol Lett* 57 (2015), 853–860.
7. K.L. Wong and C.Y. Tsai, Combined-type triple-wideband LTE tablet computer antenna, *Microw Opt Technol Lett* 57 (2015), 1262–1267.
8. Available at: <http://www.ansys.com/staticassets/ANSYS/staticassets/resource/library/brochure/ansys-hfss-brochure-16.0.pdf>, 2015, ANSYS HFSS, Ansoft Corp., Pittsburgh.
9. Y.L. Ban, Y.F. Qiang, Z. Chen, K. Kang, and J.H. Guo, A dual-loop antenna design for hepta-band WWAN/LTE metal-rimmed smartphone applications, *IEEE Trans Antenna Propag* 63 (2015), 48–58.
10. K. L. Wong and C. Y. Tsai, Small-size stacked inverted-F antenna with two hybrid shorting strips for the LTE/WWAN tablet device, *IEEE Trans Antenna Propag* 62 (2014), 3962–3969.
11. K.L. Wong and W.C. Wu, Very-low-profile hybrid open-slot/closed-slot/inverted-F antenna for the LTE smartphone, *Microw Opt Technol Lett* 58 (2016), 1572–1577.